Analysis of Experimental Ice Shedding Events on a Propeller at the NASA Glenn Icing Research Tunnel

James E. Frantz[1]
NASA Glenn Research Center, Cleveland, OH, 44135, United States

Christopher Giuffre[2]
HX5, LLC, Brook Park, OH, 44135

Paul H. von Hardenberg[3]
NASA Glenn Research Center, Cleveland, OH, 44135, United States

The aerospace industry is interested in the development and certification of Advanced Air Mobility (AAM) transportation vehicles. However, shedding of accreted ice on propellers poses a hazard for the future of AAM as they pursue all-weather operations including flight into icing conditions. An experimental study has been conducted in NASA's Icing Research Tunnel to simulate a propeller in axial flow. This test produced highspeed videos of ice shedding events. A method for analyzing these videos has been developed to identify the locations of each shedding event, including the span locations and the angular positions, using a computer script and user inputs. The data was then analyzed to evaluate the patterns in the span locations and the randomness in the angular positions. The variance of the user's graphical inputs is also evaluated, showing that this method produces a data set with a high level of accuracy that is suitable for future analyses.

I. Nomenclature

IRT	=	NASA Glenn Research Center Icing Research Tunnel
AAM	=	Advanced Air Mobility
MVD	=	Median Volumetric Diameter
LWC	=	Liquid Water Content
ARIES	=	AAM Rotor Icing Evaluation Studies
r	=	radial distance
R	=	propeller tip radius
a	=	semi-major axis of an ellipse
b	=	semi-minor axis of an ellipse
β	=	angle between the camera plane and propellor disk
x	=	pixel coordinate value in the x direction
y	=	pixel coordinate value in the y direction
h_0	=	x value for largest ellipse centroid
k_0	=	y value for largest ellipse centroid
h	=	x value for ellipse centroid
k	=	y value for ellipse centroid

[1] Student Trainee (Engineering), Icing Branch, 21000 Brookpark Rd., MS 11-2, AIAA Student Member.
[2] Aerospace Engineer, 21000 Brookpark Rd. Cleveland, OH, 44135
[3] Research Aerospace Engineer, Icing Branch, 21000 Brookpark Rd., MS 11-2.

II. Introduction

As the aerospace industry continues to innovate on propulsor designs to drive forward novel concepts and vehicle configurations, the danger posed by the shedding of ice remains an operational safety concern. With the advent of new open rotor concepts, it is critical to better understand the intersection of icing condition and the onset of shedding as this will drive both airframe safety measures as well as sizing of critical components within the propulsion unit. Ice shedding also remains a necessary consideration in the design of ducted propulsion units, however, the ability of the nacelle to contain shed ice mitigates the potential safety risks to the airframe. While the trajectory of ice shed from a horizontal tail rotor [1] has been studied, there has yet to be a systematic parametric sweep of ice shedding from rotating components conducted by NASA.

Unlike the field of ice adhesion measurement where the current literature covers a wide swath of icing conditions and substrates [2], the published data sets for ice shedding from rotating components is much smaller. The work done by Fortin and Perron [3] used an untwisted NACA 0012 and recorded the position of shedding events as a function of temperature which for a singular cloud condition can be interpreted as a parametric study based around freezing fraction. While the number of conditions presented are limited, it provides a well characterized data set on a simple geometry that has been used to develop analytical shedding models based on the body stresses induced in the ice during rotation. Another commonly cited shedding study is the work done at Penn State University during the development of the Adverse Environments Rotor Test Stand (AERTS), which captured several shedding events under a wider range of conditions [4]. For this work a slightly twisted NACA 0015 airfoil was used, and while shedding was observed across a wide range of icing conditions, there are large gaps between the conditions which had shedding events. These gaps in conditions that produced shedding events does not limit the usefulness of the data set to developing shedding models but makes it difficult to understand the role icing condition has on promoting shedding. Lastly, another ice shedding test campaign at the AERTS facility was conducted using a NACA 0012 airfoil where a single icing condition was tested with various accretion times [5].

To better understand ice shedding, the NASA Glenn Research Center has conducted tests evaluating an electric vertical takeoff and landing (eVTOL) propeller in forward flight [6]. A test entry was completed in January 2024 with a focus on gathering ice shedding data and evaluating icing scaling techniques for propellers. This paper presents an analysis of the ice shedding data from that test and covers a new method to produce accurate data of the shedding locations using highspeed camera footage and user input to calculate both the span location and angular position of each shedding event.

III. Methodology

A. Experimental Setup

The data for this analysis was collected during a 2024 test entry in the NASA Icing Research Tunnel (IRT). The IRT is a closed-loop, atmospheric wind tunnel with a 6 ft by 9 ft cross section for the test section. It has the ability to operate at wind speeds of 50 to 325 knots with temperatures between 10 ºC and -35 ºC. A schematic of the tunnel is shown in Fig. 1 [7].

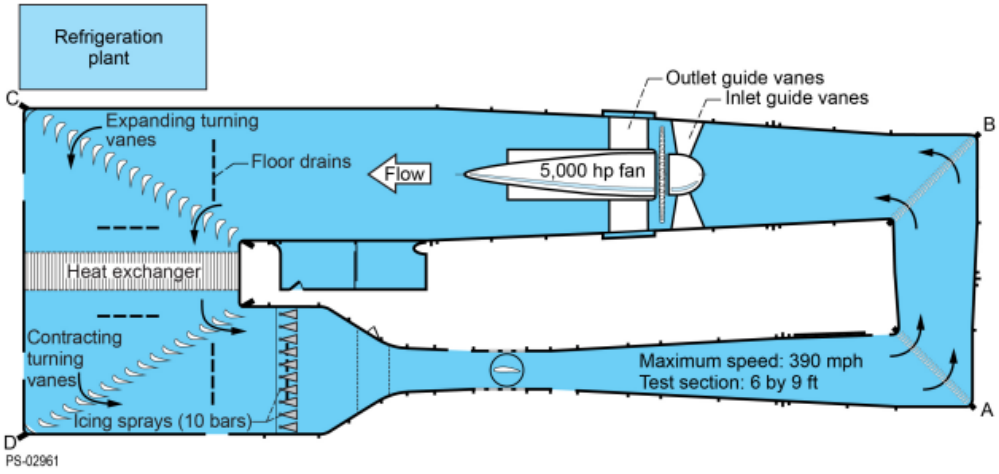

Fig. 1 A schematic of the IRT from the 2019 calibration report [7].

The position of the test article in Fig. 1 is denoted by the circled airfoil. An image of the propeller test stand installed in the IRT with the 36 in diameter blades is shown in Fig. 2 [6]. This test stand was designed to study ice accretion on electrically driven propellers and could be outfitted with different blade sizes. The blades for this experiment included 24, 28, and 36 in diameter propellers. Using a NACA 0012 airfoil, the blade twist and chord distributions were inspired by NASA's Computationally Optimized Proprotor [8]; however, some slight deviations were necessary for manufacturing feasibility purposes. The final twist and chord distributions for the three propellers can be found in Ref. [6]. During this test entry, the propeller was driven in a forward flight (axial flow) configuration as shown in Fig. 2.

Fig. 2 Image of the test stand outfitted with the 36-inch diameter blades in the IRT [6].

For this analysis, the data collected is from the 28 in and 36 in diameter propeller blades. The test conditions for each of the experiments is shown below in Table 1. Ice shapes for each reported spray condition were gathered, however since the analysis conducted in this work does not take the ice shape into account they are not presented in this work.

Table 1 Test Conditions

Run	Blade Diameter (in)	Propeller Speed (RPM)	Tunnel Velocity (knots)	Total Temperature (°C)	MVD (μm)	LWC (kg/m^3)	Time Until 1st Shed (min)
RA3794	36	996	80	-6.3	16	1.20	7.36
RA3797	28	1394	87	-6.0	15	1.20	7.23
RA3799	28	1394	87	-9.0	15	1.20	5.83
RA3802	28	1394	87	-9.0	15	1.20	6.05
RA3803	28	1763	110	-10.3	15	1.20	4.03

B. Data Collection

The data for this experiment was collected in the form of highspeed videos. These videos were taken from a Phantom v2640 camera recording at 3000 frames per second above the tunnel looking through a window panel located in the ceiling. It was located approximately 3 ft above the centerline of the test section and approximately 6.5 ft upstream from the propeller plane of rotation, as shown in Fig. 3.

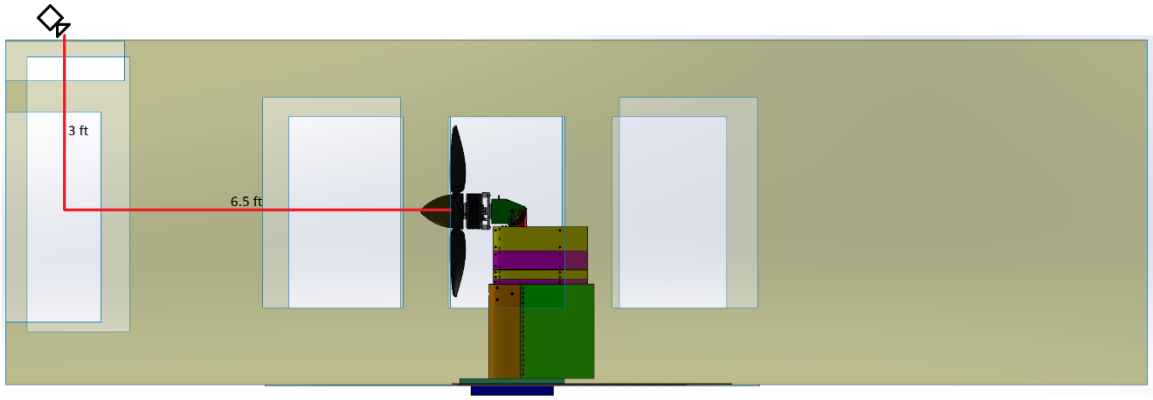

Fig. 3 Schematic of the tunnel showing the camera location relative to the test stand.

The experiment began by collecting calibration videos of the propellers running at 100 rpm with six calibration dots placed on an individual blade at known radial locations of r/R = 0.4, 0.5, 0.6, 0.7, 0.8, and 0.9, where r/R is the radial location normalized by the blade tip radius. This allowed for calibration of the locations r/R = 0.4 to 1.0 for each of the propellers since the camera and test stand remained in the same location for the icing tests. Images showing a frame from each of the calibration videos is shown below in Fig. 4.

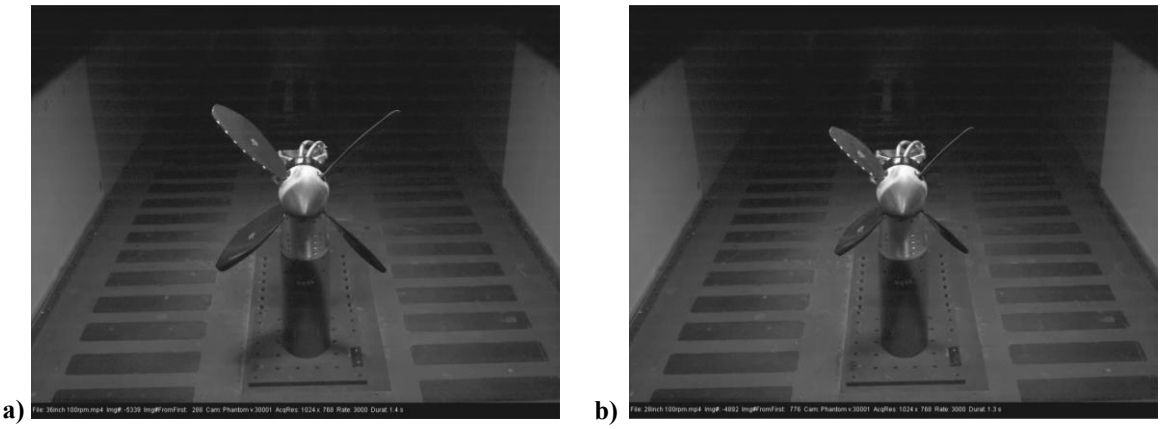

Fig. 4 Images showing the propeller blades with calibration dots on the 36-inch (a) and 28-inch (b) diameter propeller.

During a typical icing run, the propeller was operated at the target RPM and tunnel speed for several minutes until the freestream total air temperature reached a steady state at the target temperature for that run. After achieving steady state conditions, the propeller was operated for 30 seconds before introducing the icing cloud to acquire baseline performance data. The icing spray would continue for the target duration of that run or until a major shedding event resulted in vibrations that exceeded their predefined limit. Shedding events were identified by sudden spikes in vibrations or by abrupt drops in required power to the motor. After a shedding event occurred, the high-speed cameras were manually triggered to record several seconds before and after the shedding event. A collection of frames in chronological order shows a shed event in Fig. 5.

a) One frame (0.33 ms) before shedding occurs.

b) Initial shedding frame.

c) Five frames (1.67 ms) after initial shedding frame.

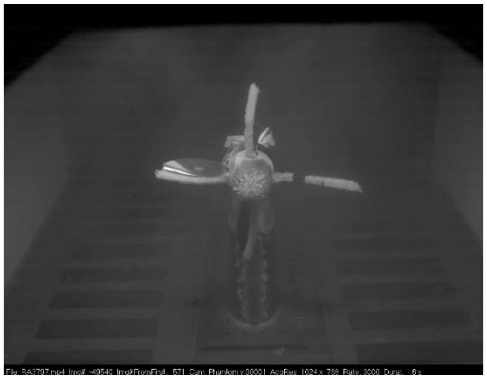

d) Ten frames (3.33 ms) after initial shedding frame.

Fig. 5 A series of frames showing a shedding event on the 28-inch diameter propeller.

C. Data Analysis

The goal of this analysis was to create a numerical data set showing the shedding locations with high accuracy from the highspeed videos. To accomplish this, a MATLAB script was written to process the videos. The process begins by reading the calibration video frame by frame over one complete rotation of the propeller and converting each frame to greyscale. Next, the pixel values of each frame are subtracted from those of the preceding frame, and the resulting difference images are overlaid onto one another. Finally, the composite image is brightened to produce the result shown in Fig. 6

Fig. 6 Calibration image created from the calibration video (28-inch diameter propeller assembly).

This image is then shown to the user, and a set of crosshairs are used to manually selects at least 5 points around the circumference of the propeller which can now be clearly observed by the transition from white to grey in Fig. 6. These points are then used to estimate an ellipse that fits the points by passing them to the fit_ellipse function from the MATLAB file exchange [9]. This function uses the least squares method to estimate the ellipse for the selected points and returns values for the centroid coordinates and the semi-major, a, and semi-minor, b, axes lengths.

To develop a model for finding the inner ellipses for each r/R corresponding to a calibration dot, an un-lightened image of the overlayed frames is used in a repetitive method similar to the method above, by manually selecting the inner ellipses created by each of the calibration dots and fitting them with ellipses. This process of manually selecting points on the inner ellipses only needs to be completed once for each propeller and is used to create an array of the centroid coordinates which is then implemented to calculate the offset of the centroid locations from the center of rotation of the propeller. This offset is caused by the location of the camera focal point not being exactly in the center of the propeller. Once this array is created for each blade diameter, it does not need to be recalculated when rerunning the code, and the inner calibration ellipses for every 10% span r/R = 0.3 to r/R = 0.9 are automatically calculated after the outer ellipse is selected. These calculations are performed and presented to the user to verify the calibration before calculating the shedding locations.

Since the camera is located in the ceiling of the tunnel, the camera perspective is not parallel to the propeller axis of rotation. As such, the first step when automatically calculating the inner ellipses for each r/R location is to use the semi-major axis, a, and semi-minor axis, b, of the observed ellipse to calculate an estimation of the viewing angle between the camera and the propeller plane, β, by using the trigonometric calculations in equations 1 through 3. A graphic showing where these variables are in relation to the experimental setup are shown in Fig. 7. In this figure, the "a" dimension in Fig 7a is the same as Fig 7b since it is known that the true propeller path is circular.

$$c = \sqrt{a^2 - b^2} \tag{1}$$

$$\alpha = \sin^{-1}\left(\frac{c}{a}\right) \tag{2}$$

$$\beta = 90° - \alpha \tag{3}$$

This angle, β, enables the calculations of the a and b axis dimensions for each r/R location using equations 4 and 5:

$$a\left(\frac{r}{R}\right) = a(1)\left(\frac{r}{R}\right) \tag{4}$$

$$b\left(\frac{r}{R}\right) = a\left(\frac{r}{R}\right)\sin(\beta) \tag{5}$$

These equations are shown to be linear functions of r/R, and the plots of the a and b values per r/R location are plotted in Fig. 8.

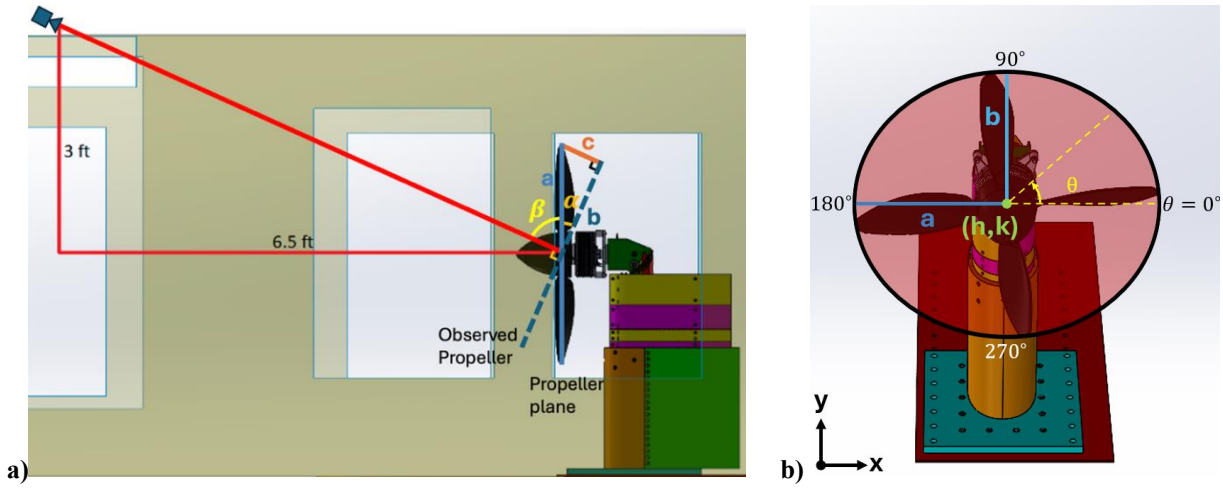

Fig. 7 Graphic showing the dimension variables for finding the camera viewing angle, $\boldsymbol{\beta}$.

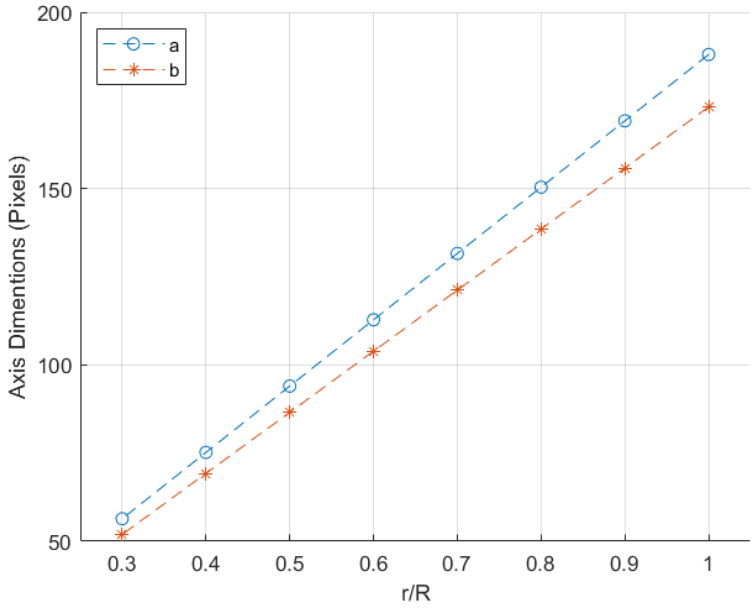

Fig. 8 Plot of a and b dimensions per r/R location.

Using the array of centroid coordinates in the observed plane from the calibration, a scaling factor for the particular centroid locations based on the selected points can be calculated from the user inputs. This happens by fitting a 2nd order polynomial to the centroid y coordinates as functions of the r/R location. This polynomial can then be used to find the new centroid y coordinate, k, shown in equation 6, where p(r/R) is the fit 2nd order polynomial and k_0 is the y coordinate of the centroid for the outer ellipse.

$$k\left(\frac{r}{R}\right) = k_0 \frac{p\left(\frac{r}{R}\right)}{p(1)} \tag{6}$$

Since equations 4 through 6 are functions of r/R, the x and y coordinate equations can also be written as functions of r/R, as shown in equations 8 and 9. Equation 7 states that since the camera is on the center line of the tunnel, there

is no variation in the centroid x coordinate, h, for the ellipses. If the camera were off the centerline, more calculations would be necessary to incorporate the values for the changing x coordinates as functions of r/R.

$$h\left(\frac{r}{R}\right) = x_0 \tag{7}$$

$$x\left(\frac{r}{R}\right) = h\left(\frac{r}{R}\right) + a\left(\frac{r}{R}\right)\cos(\theta) \tag{8}$$

$$y\left(\frac{r}{R}\right) = k\left(\frac{r}{R}\right) + b\left(\frac{r}{R}\right)\sin(\theta) \tag{9}$$

The ellipses generated from these calculations are then shown to the user on a non-lightened version or the image in Fig. 6. The image the user sees is shown in Fig. 9. This image allows the user to see the ellipses that the code calculated overlayed on the propeller with the calibration dots. The user then has the option to redo the ellipse calculations if the user decides the fitting is not tight enough.

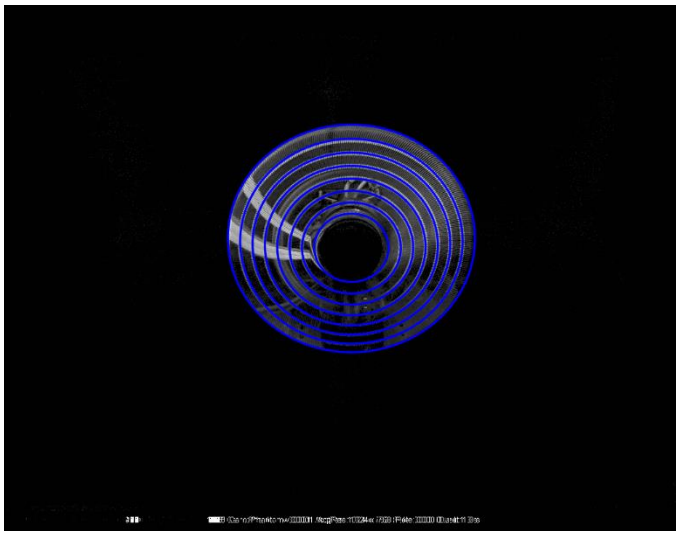

Fig. 9 Image showing the calculated ellipses for the 28-inch diameter propeller assembly.

Once the ellipse calibration calculations are confirmed, the process reads the data file containing the video frame numbers for each shed event and presents the user with the series of shed frames. If the user cannot clearly see the shed location, the user may advance the video frame by frame until the shed location is found and selected. When the shed location is selected, the pixel coordinates are used to calculate the ellipse containing the point and the angular position of the shed location by combining equations 4 through 7 into equation 10 to develop the fully parameterized equation for the ellipse solely as a function of r/R, which results in an optimization problem. This can be solved to obtain the r/R value at the selected point.

$$\min_{(r/R)}\left[\left(\frac{\left(x - h\left(\frac{r}{R}\right)\right)^2}{a\left(\frac{r}{R}\right)^2}\right) + \left(\frac{\left(y - k\left(\frac{r}{R}\right)\right)^2}{b\left(\frac{r}{R}\right)^2}\right) - 1\right] \tag{10}$$

After obtaining the r/R value of the shed, equations 4 through 7 are used to find a, b, h, and k for the new ellipse, and equations 8 and 9 are used to calculate the points for the ellipse based on the selected point at the shed location. The angle of the point relative to the right-hand horizontal, θ, can also be found. The conversion from the elliptical coordinates to the circular coordinates is $F = a_0/b_0$, where a_0 and b_0 are the semi-major and semi-minor axes respectively of the outer ellipse. The circular coordinates are given in equations 11 and 12.

$$x_{circ} = (x - h) \tag{11}$$

$$y_{circ} = F(y - k) \tag{12}$$

After the x and y points have been scaled, the angle in relation to the horizontal can be found using equation 13.

$$\theta = \tan^{-1}\left(\frac{y_{circ}}{x_{circ}}\right) \tag{13}$$

A plot showing an example of a shed point and calculated ellipses are shown in Fig. 10. Note that this is the same shedding event shown in Fig. 5.

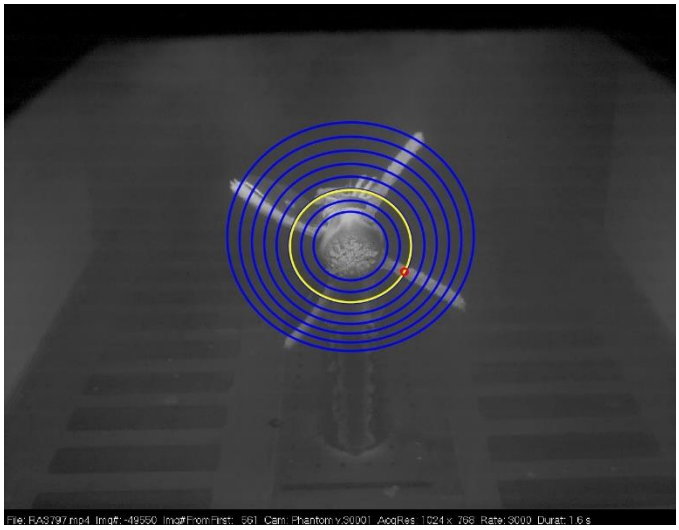

Fig. 10 Plot of the selected shed location point (red) and the calculated ellipse (yellow).

D. Discussion of the Variance

Prior to conducting analysis of the shedding events, it is critical to understand the variance in position fitting. The variance for these fittings were computed by manually selecting each of the calibration dots at four different stations in the rotation of the propeller, set so the blades are at θ= 0º, 90º, 180º and 270º as shown in Fig. 11. This allowed the calculated value of r/R on the fit ellipses to be compared to the known r/R value at each selected point. The plots for the variance check from each of the blades is shown in Fig. 12 for both the 28 in and 36 in diameter propellor blade assemblies.

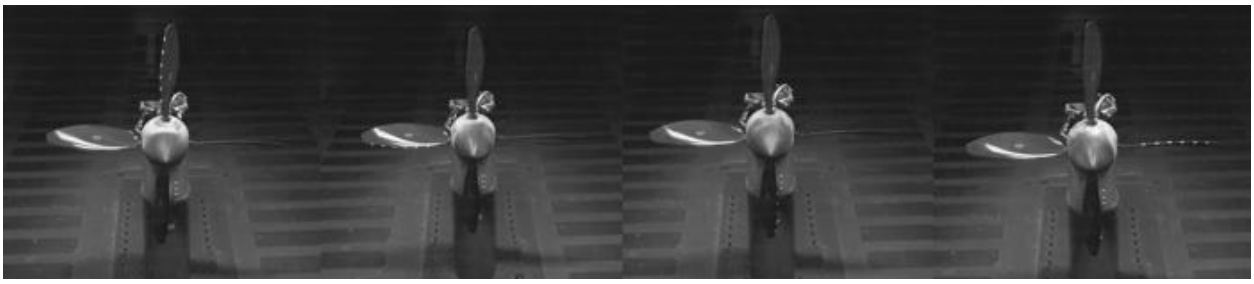

Fig. 11 Image series of the frames to receive the variance check input for the 36-inch diameter propeller assembly.

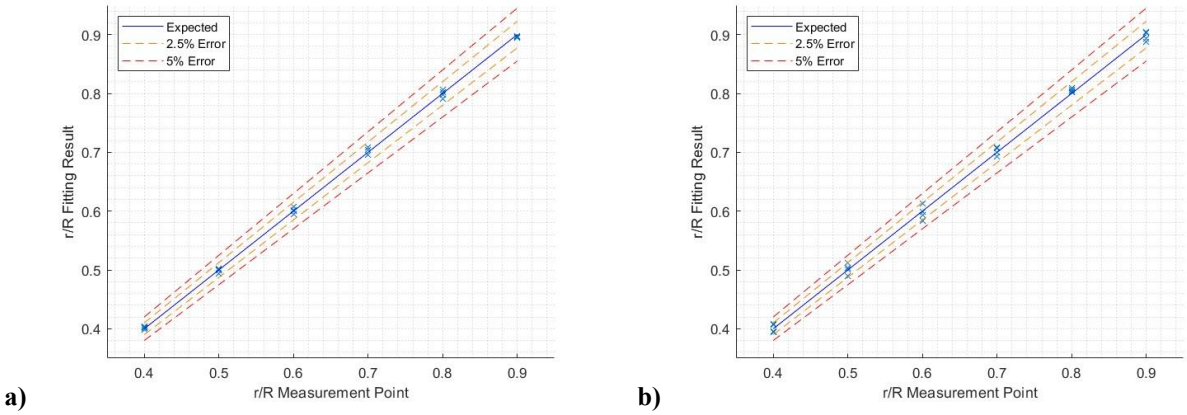

Fig. 12 Plots of the variance of user inputs for the 36-inch (a) and 28-inch (b) diameter propeller assembly.

For both sets of propellor blades studied, all of the fitting results fall very close to the expected values, shown by the solid blue line. Error bounds are included with the yellow lines bounding ±2.5% error, and the orange lines bounding ±5% error. It is shown that all the points are within the ±2.5% error lines, which is an acceptable margin. The selections for both the original ellipse fitting as well as the variance check are tracking the pixel values of the clicks, so a small amount of variance is expected and aligns with the findings. While selecting the position of a shedding event will not be the exact position of the rotating propeller, the results shown provide confidence that this method is able to recover the approximate position of the event.

IV.Results

E. Discussion of the output plots

Using the calculations for r/R for each shed event, the plots shown in Fig. 13 were generated for the 36 in and 28 in propellor blade assemblies. It is important to note that each blade was not individually tracked for this analysis, and the shed number simply implies the order of events.

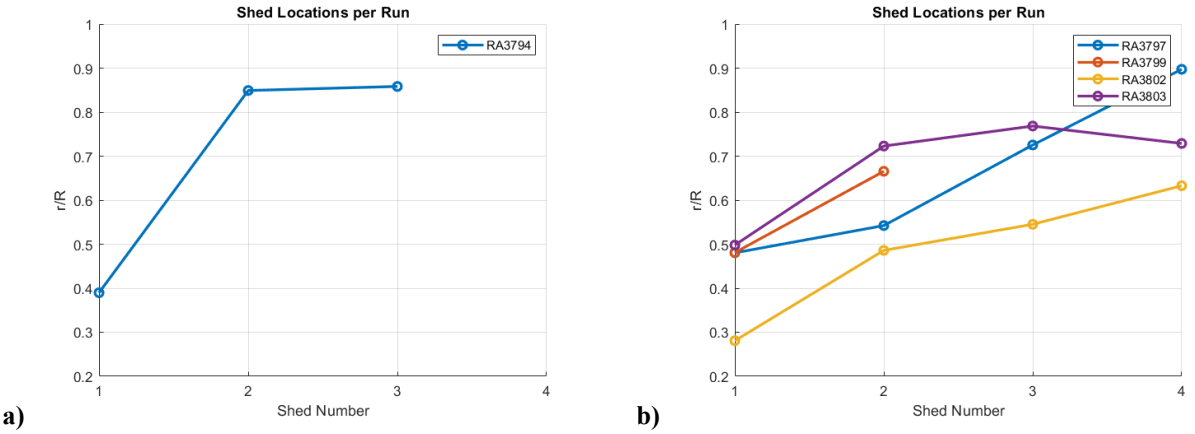

Fig. 13 Plots of the r/R locations for each shedding event per run: 36-inch (a) and 28-inch (b) diameter propeller assembly.

In these plots, it is shown that for the majority of cases, the 1st shed happens relatively inboard at r/R < 0.55 and the second shed is further outboard. The 3rd and 4th sheds appear to be more random and therefore no conclusions can be drawn from them.

The second plot generated is a polar plot of the shed locations as shown in Fig. 14. Again, each shed is numbered per given run with the colors dictating the case. These plots show the locations of the sheds in relation to the horizontal

and have been adjusted to be plotted on circles. This creates a representative view of the propellers as if viewed from directly upstream, allowing the user to check for any trends in the angular position data.

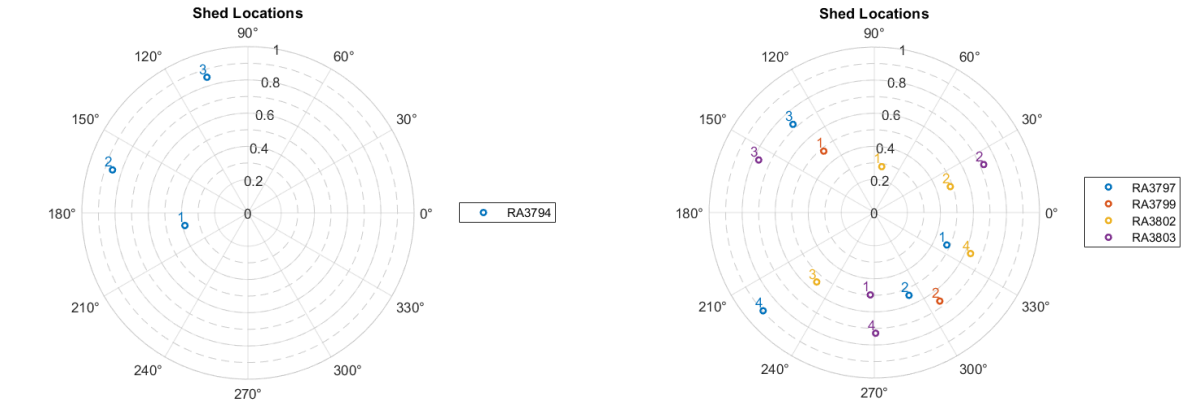

a) b)

Fig. 14 Plots of the shed locations with respect to r/R and the angle, θ, for the 36-inch (a) and 28-inch (b) diameter propeller.

The polar plots above show there is no readily noticeable pattern or grouping of the shed angles. This was expected from an axisymmetric propeller and shows that secondary effects such as gravity or the test stand geometry has negligible effect on inducing shedding events.

V.Conclusion

The methodology developed has proven its ability to create highly accurate data of the locations of shedding events. Using the test data collected during the test campaign in the NASA IRT, the analysis of the data produced by this methodology shows that patterns may start to appear for different run conditions. It is shown for the conditions tested that the first shedding event occurs below 55% span and the second shed usually occurs outboard of the first.

There is also randomness in the angular locations at which shedding occurs, as expected. This rules out any constant effects on the data which would influence many tests across conditions. It has also been shown that the data collection method produces results within a 2.5% variance between the r/R values calculated by this analysis and expected values given by the user. This validates the method and shows that it can be used to analyze more run cases and create valuable data sets that may be paired with the 3D laser scan data for further shedding analyses in the future.

VI. Acknowledgements

The authors wish to acknowledge the financial support by NASA's Revolutionary Vertical Lift Technology (RVLT) and the Advanced Air Transport Technology (AATT) projects under NASA's Advanced Air Vehicles Program (AAVP). The authors would also like to acknowledge the IRT engineers and technicians for their support which directly led to the success of this test campaign. Additionally, this study would not have been possible without the efforts of Quentin Schwinn and Jordan Salkin for all of their support with the imaging portion of this work.

VII. References

[1] Kreeger, R. E., Work, A., Douglass, R., Gazella, M., Koster, Z., and Turk, J., "Analysis and Prediction of Ice Shedding for a Full-Scale Heated Rotor," 8th AIAA Atmospheric and Space Environments Conference, 2016, AIAA2016-3443

[2] Work, A., and Lian, Y., "A critical Review of the measurement of ice adhesion to solid substrates," Progress in Aerospace Sciences, Vol 98, pp 1-26, 2018

[3] Fortin G., and Perron J., "Spinning Rotor Blade Tests in Icing Wind Tunnel," 1st AIAA Atmospheric and Space Environments Conference, 2009

[4] Brouwers, E., “The experimental investigation of a rotor icing model with shedding,” Thesis, Pennsylvania State University, 2010

[5] Schneeberger, G. M., “Ice projectile length prediction of shed ice from rotor blades,” Thesis, Pennsylvania State University, 2016

[6] Von Hardenberg, P. H., Flack, C. A. and Rigby, D. L., "Ice Shape Analysis of an eVTOL Propeller in Forward Flight at the NASA Glenn Icing Research Tunnel," *AIAA AVIATION FORUM AND ASCEND 2024*. Las Vegas, NV, July 2024.

[7] Timko, E. N., King-Steen, L. E., Van Zante, J. F., and Acosta, W. J., “NASA Glenn Icing Research Tunnel: 2019 Cloud Calibration Procedure and Results,” NASA/TM-20205009045, 2021.

[8] Zawodny, N. S., Pettingill, N. A., Lopes, L. V., and Ingraham, D, J., “Experimental Validation of an Acoustically and Aerodynamically Optimized UAM Proprotor Part 1: Test Setup and Results,” NASA/TM-20220015637, 2023.

[9] Ohad Gal (2025). fit_ellipse (https://www.mathworks.com/matlabcentral/fileexchange/3215-fit_ellipse), MATLAB Central File Exchange. Retrieved February 18, 2025.